PCCP

PAPER

View Article Online
View Journal | View Issue

Published on 23 January 2017. Downloaded by University of Massachusetts - Amherst on 19/07/2017 22:07:59.

Cite this: *Phys. Chem. Chem. Phys.*, 2017, **19**, 4809

Triplet exciton dissociation and electron extraction in graphene-templated pentacene observed with ultrafast spectroscopy†

Thomas J. McDonough,[a] Lushuai Zhang,‡[b] Susmit Singha Roy,§[b] Nicholas M. Kearns,[a] Michael S. Arnold,[b] Martin T. Zanni*[a] and Trisha L. Andrew‡[ab]

Received 20th September 2016,
Accepted 20th January 2017

DOI: 10.1039/c6cp06454j

rsc.li/pccp

We compare the ultrafast dynamics of singlet fission and charge generation in pentacene films grown on glass and graphene. Pentacene grown on graphene is interesting because it forms large crystals with the long axis of the molecules "lying-down" (parallel to the surface). At low excitation fluence, spectra for pentacene on graphene contain triplet absorptions at 507 and 545 nm and no bleaching at 630 nm, which we show is due to the orientation of the pentacene molecules. We perform the first transient absorption anisotropy measurements on pentacene, observing negative anisotropy of the 507 and 545 nm peaks, consistent with triplet absorption. A broad feature at 853 nm, observed on both glass and graphene, is isotropic, suggesting hole absorption. At high fluence, there are additional features, whose kinetics and anisotropies are not explained by heating, that we assign to charge generation; we propose a polaron pair absorption at 614 nm. The lifetimes are shorter at high fluence for both pentacene on glass and graphene, indicative of triplet–triplet annihilation that likely enhances charge generation. The anisotropy decays more slowly for pentacene on graphene than on glass, in keeping with the smaller domain size observed *via* atomic force microscopy. Coherent acoustic phonons are observed for pentacene on graphene, which is a consequence of more homogeneous domains. Measuring the ultrafast dynamics of pentacene as a function of molecular orientation, fluence, and polarization provides new insight to previous spectral assignments.

1 Introduction

The loss of high energy photons to thermalization presents a fundamental limitation to the efficiency of single junction photovoltaics.[1] One method to surpass this limit is to utilize organic semiconductors that can generate two electron–hole pairs for each incident photon through singlet fission.[2] In this spin-conserving process, a singlet exciton interacts with a nearby ground state molecule to generate two separate triplet excitons.[3–5] Photovoltaic devices and photodetectors utilizing pentacene have been developed with internal quantum efficiencies nearing 200%.[6–9] Further improvements in device efficiency will be aided by a more complete understanding of the effects of morphology on exciton and charge dynamics, particularly the identification of competing loss channels.[10]

It has recently been demonstrated that devices made with graphene-templated pentacene have twice the exciton diffusion length (~100 nm) and five times the maximum power conversion efficiency (~4%) of devices on glass.[11] Devices made with graphene-templated pentacene have domains that are rotated nearly 90° relative to pentacene grown on glass (Fig. 1d). Domain orientation in the device can be beneficial for charge separation and collection due to anisotropic charge mobility.[12,13] This rotation provides improved charge mobility in the direction normal to the device plane, enhancing charge collection.[11]

The graphene-templated devices also likely benefit from increased domain size and thus fewer traps. Film morphology can have a significant effect on device performance[14] and ultrafast photophysics, as has been observed in acenes (or their derivatives)

[a] *Department of Chemistry, University of Wisconsin–Madison, 1101 University Ave, Madison, WI 53706, USA. E-mail: zanni@chem.wisc.edu; Fax: +1 608 262-9918; Tel: +1 608 262-4783*

[b] *Department of Materials Science and Engineering, University of Wisconsin–Madison, 1509 University Ave, Madison, WI 53706, USA*

† Electronic supplementary information (ESI) available: Calculation of excitation density; comparison of transient absorption spectra for pentacene on graphene with 505 and 565 nm excitation; comparison of transient absorption spectra at low and high fluence; representative spectral slices and corresponding fits to high fluence transient absorption data using only peaks obtained from low fluence fits; temperature-dependent absorption spectra and method; additional transient heating fit results. See DOI: 10.1039/c6cp06454j

‡ Current address: Department of Chemistry, University of Massachusetts Amherst, 710 N Pleasant St, Amherst, MA 01003, USA.

§ Current address: Applied Materials, Inc., 3330 Scott Blvd, Santa Clara, CA 95054, USA.

Published on 23 January 2017. Downloaded by University of Massachusetts - Amherst on 19/07/2017 22:07:59.

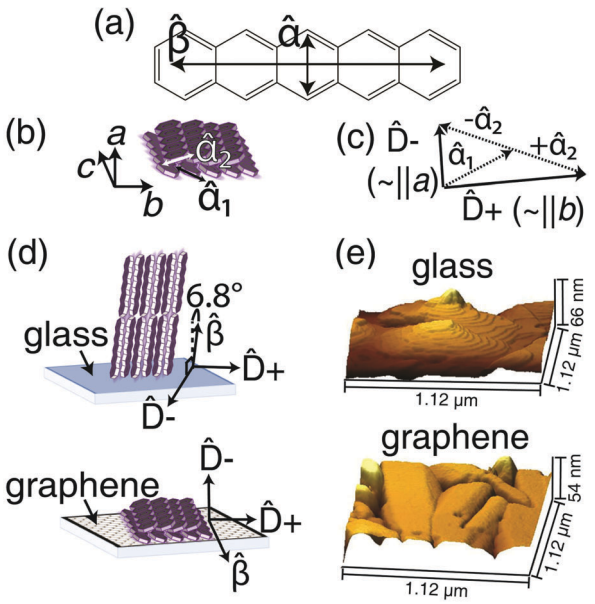

Fig. 1 (a) Pentacene molecular structure. The unit vectors $\hat{\alpha}$ and $\hat{\beta}$ correspond to the orthogonal transition dipole moment directions of the S_0–S_1 (monomer) and S_0–S_3/T_1–T_N transitions, respectively. (b) Pentacene crystal with approximate crystallographic axes labelled. (c) Schematic vector summation giving rise to the directions of the longer ($\hat{D}_+$ or $\sim\|b$) and shorter ($\hat{D}_-$ or $\sim\|a$) wavelength Davydov components in the crystal. (d) Orientation of pentacene on glass (top) and graphene (bottom) with relevant transition dipole moment directions indicated. (e) 3D AFM topography images of pentacene on glass (top) and graphene (bottom).

in single crystals,[15] polycrystalline thin films,[16,17] amorphous thin films,[18] and nanoparticles.[19,20] Control of the domain size is important because charge carriers must reach a donor–acceptor interface without becoming trapped at sites where charge separation cannot occur.[21] As measured *via* atomic force microscopy, pentacene deposited on glass exhibits scattered terrace-like domains of $\sim$200 nm^2 area with the molecules oriented almost normal to the surface ($\theta = 6.8^\circ$), *i.e.* "standing-up" (Fig. 1d and e; top).[22] It has been suggested that the terrace-like domains provide a large surface area over which defects can exist.[23] When pentacene is instead deposited on graphene, smoother, more densely packed rectangular domains with lengths reaching up to 1 μm are formed with the long axis of the molecules parallel to the surface, *i.e.* "lying-down" (Fig. 1d and e; bottom).[22] Nanosecond surface photoresponse measurements have indicated that the graphene layer efficiently extracts electrons from pentacene.[24]

Given that the device performance of pentacene grown on graphene is much different than when grown on glass, we investigate whether the femtosecond and picosecond photoexcitation dynamics are different as well. Orientation is also important for interpreting spectroscopy, because signal strength scales with the degree of overlap between the transition dipole moment(s) and the incident light polarization. Thus, pentacene on graphene will exhibit different spectroscopic intensities than the more commonly studied system, pentacene on glass, thereby providing additional data on band assignments and kinetics.

2 Experimental

2.1 Sample preparation

Pentacene (sublimed grade) was obtained from TCI and used as received. Polycrystalline pentacene films of 100 nm thickness were prepared by thermal evaporation onto O_2 plasma treated glass or monolayer graphene-covered glass substrates at a rate of 0.3 Å s^{-1} in a vacuum of below 1 $\times$ 10^{-6} Torr. Graphene monolayers were grown *via* chemical vapor deposition (CVD) and transferred to glass according to a previously published procedure.[22,24] Sample topography was measured with an Agilent 5510 atomic force microscope. Absorption (1-R-T) spectra were measured with an Evolution 220 UV-visible spectrophotometer with an ISA 220 integrating sphere under reflectance and transmittance mode.

2.2 Transient absorption spectroscopy

Transient absorption spectra at low fluence (2 μJ cm^{-2} per 20 nm of bandwidth; corresponding to wavelength-integrated excitation densities of 8.2 $\times$ 10^{16} and 5.3 $\times$ 10^{16} cm^{-3} for pentacene on glass and graphene, respectively [see Fig. S1, ESI†]) were conducted using the 1040 nm, 400 fs output of a Spectra Physics Spirit system operating at 100 kHz. We do not see any evidence of heating due to the high repetition rate, as there is no residual intensity that carries over from one laser pulse to the next. The fundamental was split into pump and probe lines for separate continuum generation *via* focusing into 4 mm undoped yttrium aluminum garnet (YAG) crystals. The pump spectrum spanned a 608–765 nm range. The time between the pump and probe pulses was controlled by a mechanical delay stage (National Aperture, Inc.). The probe beam was dispersed with a Princeton Systems Acton SpectraPro SP-2150 spectrometer and collected on a linear array camera (e2v AViiVA EM4).

Transient absorption measurements at high fluence (50 μJ cm^{-2}; corresponding to wavelength-integrated excitation densities of 1.9 $\times$ 10^{18} and 1.7 $\times$ 10^{18} cm^{-3} for pentacene on glass and graphene, respectively [see Fig. S1, ESI†]) were conducted using the 800 nm, 40 fs output of a 1 kHz regeneratively amplified Ti:Sapphire laser system (Coherent Legend Elite). Approximately 1.5 W of the amplifier output was directed to the transient absorption experiment, 90% of which was used to pump a home-built two-pass non-collinear optical parametric amplifier (NOPA) to produce $\sim$20 nm full width at half maximum (FWHM) pump pulses in the 505–565 nm range. The transient absorption spectra exhibited no significant change with pump frequency in this range (see Fig. S2, ESI†). The other 10% of the fundamental was focused into a 3 mm sapphire crystal to generate a supercontinuum probe. The time between the pump and probe pulses was controlled by a mechanical delay stage (Aerotech). A small portion of the probe beam was split off with a neutral density (ND) filter to create a reference beam. The probe and reference were dispersed by a home-built spectrometer onto separate linear CCD arrays. Laser shots were averaged on the arrays for 300 ms (300 laser shots) using mechanical shutters on the pump and probe to obtain one transient absorption spectrum at a given time point. Data sets

 This journal is © the Owner Societies 2017

Published on 23 January 2017. Downloaded by University of Massachusetts - Amherst on 19/07/2017 22:07:59.

were an average of typically twenty such spectra for each time point.

In the low (high) fluence experiment, a $\lambda/2$ waveplate was used to control the probe (pump) polarization. Kinetics were collected at a relative angle of 45° (the magic angle for a sample in which the transition dipole moments reorient in only two dimensions; see Section 3, Theoretical) between the pump and probe polarizations. Anisotropy measurements are the average of three trials of consecutive scans at parallel and perpendicular pump–probe polarization.

For both low and high fluence measurements, the instrument response function was determined by convolution of a Gaussian with the exponential decays used to fit the kinetics (see Section 4, Results). In both cases, the instrument response function was determined to be ~100 fs FWHM.

3 Theoretical

Below, we report the first transient absorption anisotropy measurements of pentacene on glass and graphene. Anisotropy in materials isotropic in three dimensions is a common measurement in the literature. Here, the transition dipole moments only reorient in two dimensions because the molecules have a fixed orientation relative to the sample plane. In this section, we derive the equations to help interterpet our anisotropy measurements in two dimensions.

We follow the formalism presented by Hamm and Zanni for two coupled transition dipoles in three dimensions, but modify the equations to the case where the angles of the transition dipoles relative to the substrate plane are fixed.[25] We consider two coupled transition dipoles, $\hat{\alpha}$ and $\hat{\beta}$, in the molecular frame with a fixed angle between them, $\theta_{\alpha\beta}$ (Fig. 2, inset). We begin by aligning the molecular frame with the laboratory frame such that $\hat{\alpha}$ lies along the z-axis and $\hat{\beta}$ lies in the (x,z)-plane:

$$\hat{\alpha} = (0,\ 0,\ 1)$$
$$\hat{\beta} = (\sin\theta_{\alpha\beta},\ 0,\ \cos\theta_{\alpha\beta}). \tag{3.1}$$

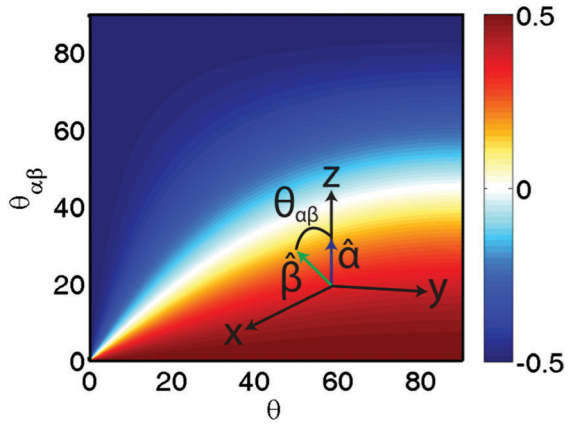

Fig. 2 Dependence of two-dimensional anisotropy on θ and $\theta_{\alpha\beta}$. (inset) Orientation of two coupled transition dipoles, $\hat{\alpha}$ and $\hat{\beta}$.

Next, we use Euler angles and rotation matrices to rotate the molecular frame against the laboratory frame. We will perform two counterclockwise rotations: one through an angle θ around x and then another through an angle ϕ around z. This transformation corresponds to the overall rotation matrix:

$$R(\theta,\phi) = \begin{pmatrix} \cos\phi & \sin\phi & 0 \\ -\sin\phi & \cos\phi & 0 \\ 0 & 0 & 1 \end{pmatrix}\begin{pmatrix} 1 & 0 & 0 \\ 0 & \cos\theta & \sin\theta \\ 0 & -\sin\theta & \cos\theta \end{pmatrix}$$
$$= \begin{pmatrix} \cos\phi & \cos\theta\sin\phi & \sin\theta\sin\phi \\ -\sin\phi & \cos\theta\cos\phi & \cos\phi\sin\theta \\ 0 & -\sin\theta & \cos\theta \end{pmatrix}. \tag{3.2}$$

Following this rotation, $\hat{\alpha}$ and $\hat{\beta}$ are transformed into:

$$\hat{\alpha}' = R(\theta,\phi)\hat{\alpha} = \begin{pmatrix} \sin\theta\sin\phi \\ \cos\phi\sin\theta \\ \cos\theta \end{pmatrix}$$
$$\hat{\beta}' = R(\theta,\phi)\hat{\beta} = \begin{pmatrix} \cos\theta_{\alpha\beta}\sin\theta\sin\phi + \cos\phi\sin\theta_{\alpha\beta} \\ \cos\phi\cos\theta_{\alpha\beta}\sin\theta - \sin\phi\sin\theta_{\alpha\beta} \\ \cos\theta\cos\theta_{\alpha\beta} \end{pmatrix}. \tag{3.3}$$

We can calculate the orientational dependence of the linear absorption spectrum:

$$I = \left\langle (\hat{X}\cdot\hat{\alpha}')(\hat{X}\cdot\hat{\alpha}')\right\rangle = p_0{}' \int \mathrm{d}\Omega' \sin^2\theta\sin^2\phi$$
$$= \frac{1}{2\pi}\int_0^{2\pi}\mathrm{d}\phi\sin^2\theta\sin^2\phi = \frac{1}{2}\sin^2\theta, \tag{3.4}$$

where $\hat{X}$ corresponds to the laser polarization. We integrated over ϕ to average the molecular frame relative to the (x, y)-plane of the laboratory frame, but the tilt of the molecular frame relative to the (x, y)-plane, θ, is fixed. For the transient absorption anisotropy measurement, we must calculate the orientational factors in parallel and perpendicular pump–probe polarizations:

$$I_{\parallel} = \left\langle (\hat{X}\cdot\hat{\alpha}')(\hat{X}\cdot\hat{\alpha}')\left(\hat{X}\cdot\hat{\beta}'\right)\left(\hat{X}\cdot\hat{\beta}'\right)\right\rangle$$
$$= \frac{1}{32}\sin^2\theta\left(5 - 6\cos 2\theta\cos^2\theta_{\alpha\beta} + \cos 2\theta_{\alpha\beta}\right)$$
$$I_{\perp} = \left\langle (\hat{Y}\cdot\hat{\alpha}')(\hat{Y}\cdot\hat{\alpha}')\left(\hat{X}\cdot\hat{\beta}'\right)\left(\hat{X}\cdot\hat{\beta}'\right)\right\rangle$$
$$= -\frac{1}{32}\sin^2\theta\left(-7 + \cos 2\theta + \cos 2\theta_{\alpha\beta}(5 + \cos 2\theta)\right). \tag{3.5}$$

We plot the anisotropy, $S = (I_{\parallel} - I_{\perp})/(I_{\parallel} + I_{\perp})$, as a function of θ and $\theta_{\alpha\beta}$ in Fig. 2. Here, we have ignored any reorientation of the dipoles that could occur during the population time, T, between the pump and probe pulses.[26] In our system, reorientation can occur due to energy transfer between crystal

Published on 23 January 2017. Downloaded by University of Massachusetts - Amherst on 19/07/2017 22:07:59.

domains, which would cause the anisotropy value to decay towards zero.[27]

4 Results

4.1 Absorption spectra of pentacene on glass and graphene

Because they have the same domain structure, we compare pentacene on glass to pentacene on graphene, the former of which has been studied previously.[23,28–37] Shown in Fig. 3 are the absorption spectra of pentacene on glass and graphene for the same film thickness of 100 nm. The transition dipole directions for the singlet and triplet transitions are shown in Fig. 1a. In the solid state, the S_0–S_1 transition undergoes Davydov splitting[38] to generate a longer wavelength component (681 nm) oriented roughly parallel to the b axis ($\hat{D}_+$) and a shorter wavelength component (630 nm) oriented roughly parallel to the a axis ($\hat{D}_-$) (Fig. 1b and c). Each of these fundamental transitions exhibit vibrational sidebands at 585 and 551 nm.[39] The S_0–S_3 transition does not exhibit Davydov splitting and occurs below 500 nm, peaking at 335 nm.[40] On graphene, the 630 nm peak is not well-resolved. This is consistent with the orientation of the $\hat{D}_-$ transition dipole moment out of the plane of the substrate on graphene *versus* its orientation in the plane of the substrate on glass (Fig. 1d). Thus, this transition has a different probability for absorbing light incident normal to each substrate. The S_0–S_1 transition dipole moments of pentacene on glass are more favourably oriented to absorb laser light at normal incidence than they are for pentacene on graphene. In contrast, the S_0–S_3 absorption is enhanced on graphene due to its more favourable orientation along the long axis of the molecule.[11]

4.2 Transient absorption spectra with Gaussian fits

Most previously reported transient absorption experiments for pentacene on glass used moderately high fluences ($\geq$50 μJ cm^{-2}).

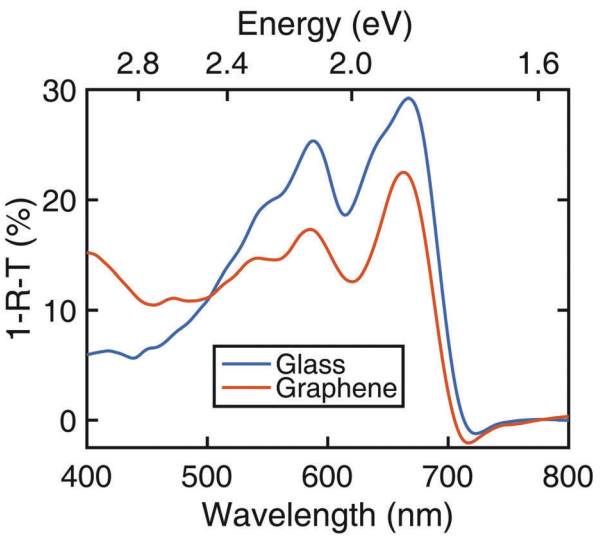

Fig. 3 Percent absorption for pentacene on glass (blue) and graphene (red).

We repeat these experiments below as a control experiment (Fig. 5), but, before turning to that data, we first report transient absorption measurements at a low fluence of 2 μJ cm^{-2}, as shown in Fig. 4a and b, for pentacene on glass and graphene. We fit the low fluence transient absorption spectra of pentacene on glass (graphene) at T = 3.3 ps to the sum of six (eight) Gaussians. The fit parameters are given in Table 1. The spectra fit well with a common set of b (center wavelength) and c (FWHM = $2(2\ln 2)^{1/2}c$) parameters. Thus, even though the spectra are visually very different from one another, they are mostly composed of the same features, albeit with different intensities.

The 551, 585, 630, and 681 nm peaks are due to bleaching of the ground state.[41] The 630 nm bleach is only observed for pentacene on glass, not on graphene, consistent with it being less prominent in the linear absorption spectrum on graphene (Fig. 3). The 551 and 585 nm bleaches are not observed for pentacene on graphene because of spectral overlap with strong absorptions at 507 and 545 nm.

These 507 and 545 nm absorptions (Fig. 4b) are the most obvious differences between the spectra of pentacene on glass and graphene. On graphene, these peaks are greater than or equal to the intensity of the bleach at 681 nm; on glass, they are absent. These features are consistent with triplet formation, for the following reasons. Triplet absorption is known to occur at these frequencies for pentacene on glass.[3] The intensities of these features on glass *versus* graphene are very different because of the orientation of their transition dipoles. On glass, the long axis of the molecule is upright and so will absorb little normal incidence laser light (Fig. 1d; top), thus making the

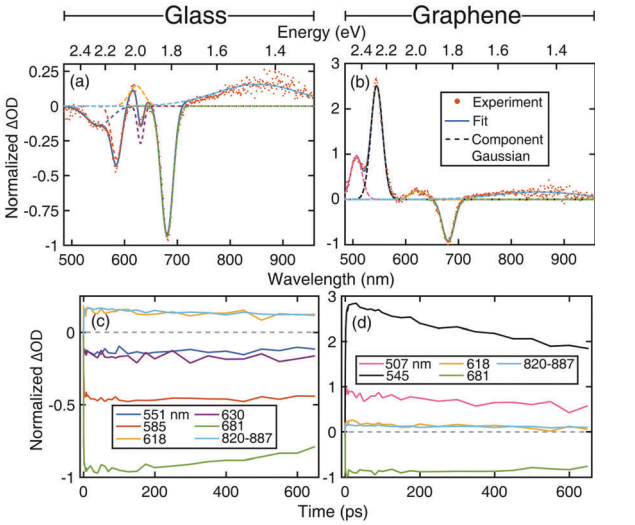

Fig. 4 Transient absorption spectra (T = 3.3 ps) at low fluence for pentacene on (a) glass and (b) graphene. The experimental spectra (red dots) are shown along with the fits (solid blue lines) and their component Gaussians (dashed lines). Corresponding transient absorption kinetics for pentacene on (c) glass and (d) graphene. The colors of the traces in (c and d) match the colors of the associated component Gaussians in (a and b). Kinetics for the peak centered at 623 nm are plotted at 618 nm to minimize the effect of overlap with the 585 and 630 nm peaks. Excitation was at 608–765 nm and 2 μJ cm^{-2} fluence.

This journal is © the Owner Societies 2017

Published on 23 January 2017. Downloaded by University of Massachusetts - Amherst on 19/07/2017 22:07:59.

Table 1 Parameters describing the component Gaussians used to fit low fluence transient absorption spectra: $\Delta OD(\lambda) = a \times \exp(-(\lambda - b)^2/(2c^2))$

b (nm)	506.6 ± 0.5	545.1 ± 0.2	551 ± 13	585 ± 1	623 ± 3	630 ± 1	680.6 ± 0.3	853 ± 6
c (nm)	10.8 ± 0.6	11.1 ± 0.4	23 ± 11	10 ± 2	14 ± 3	6 ± 2	11.3 ± 0.3	80 ± 7
a (glass)	—	—	−0.14 ± 0.03	−0.4 ± 0.1	0.15 ± 0.06	−0.3 ± 0.1	−0.94 ± 0.03	0.16 ± 0.01
a (graphene)	0.95 ± 0.04	2.5 ± 0.1	0.0 ± 0.1	0.00 ± 0.06	0.18 ± 0.03	—	−0.94 ± 0.03	0.16 ± 0.01

triplet absorption weak or not observable. On graphene, the long axis lies in the plane (Fig. 1d; bottom) and so the transition dipole is oriented favourably for absorbing normal incidence light. Triplet absorption at 545 nm has been previously observed on glass by varying the incidence angle of the probe beam 50–70° relative to the sample surface normal (as compared to our work at 0°).[23,29,33] Thus, we assign the 507 and 545 nm absorptions to triplet formation. In contrast, the 853 nm peak, which is typically assigned to triplet absorption, is inconsistent with that assignment, because it does not show any change in intensity between glass and graphene. This inconsistency is a point that we return to in the Discussion, Section 5.1. We discuss the remaining 623 nm peak in Section 4.4.

High fluence data is shown in Fig. 5a–d for representative delays at T = 0 and 900 ps. Besides the peaks observed at low fluences, the high fluence spectra contain three additional absorption features at 639, 654, and 688 nm (see Fig. S3 and S4, ESI†).

The kinetics provide insight into the fluence dependence of the dynamics. Shown in Fig. 5i–l are the kinetics for each of the individual components of the global fits. At high fluence, the bleach features at 551, 585, 630, and 672/677 nm go negative within the time resolution of the instrument and then recover with a biexponential timescale (Table 2). For most features, the recovery occurs on a few picosecond timescale, followed by a time constant greater than our longest time delay of 900 ps. In the low fluence data, the bleach also forms within the time resolution of our experiment, but the bleaches do not recover. Thus, we learn from the bleaches that the decays on a few picosecond timescale are due to multiexciton effects, since they occur at high fluence but not low fluence. The triplet state at 545 nm also exhibits multiphoton effects on the tens to hundreds of picoseconds timescale (Table 2).

4.3 Time-resolved anisotropy

Time-resolved anisotropy measurements, $S = (I_{\parallel} - I_{\perp})/(I_{\parallel} + I_{\perp})$, are shown in Fig. 6, which provide three additional insights

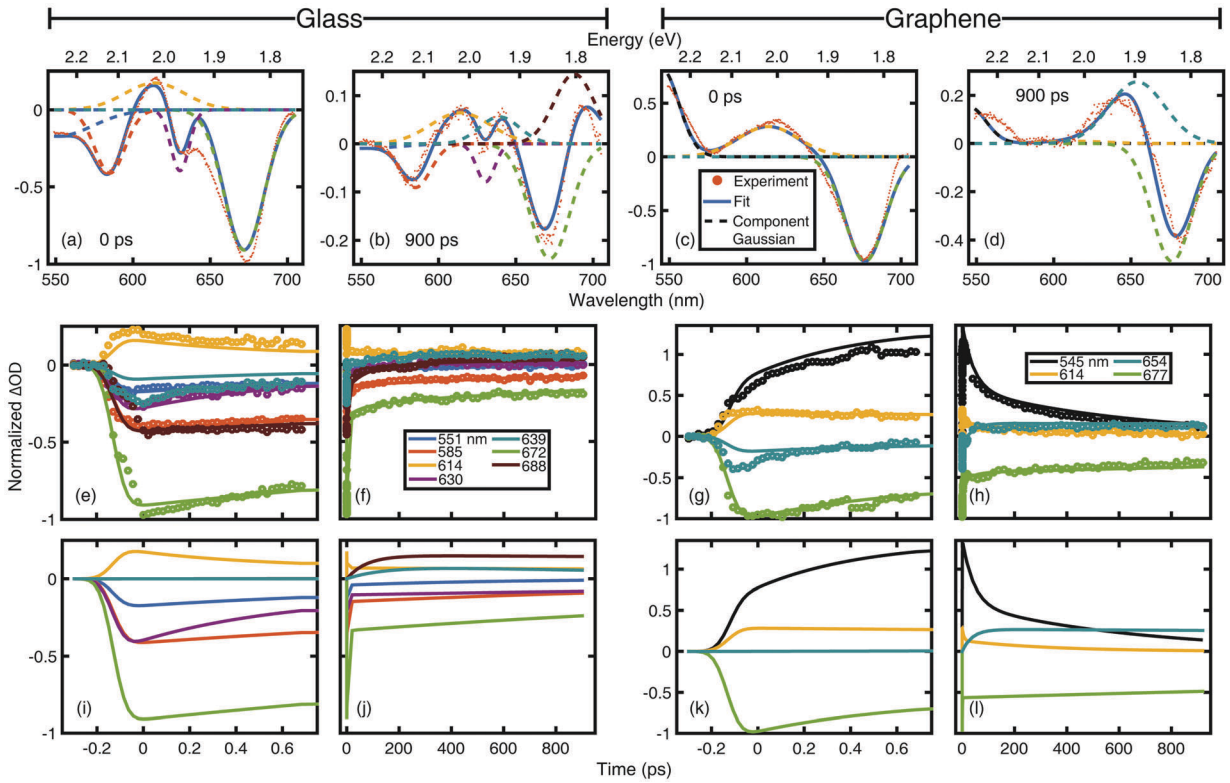

Fig. 5 Transient absorption spectra for pentacene on (a and b) glass and (c and d) graphene at T = 0 (a and c) and 900 ps (b and d). The experimental spectra (red dots) are shown along with the fits (solid blue lines) and their component Gaussians (dashed lines). Experimental kinetics for pentacene on (e and f) glass and (g and h) graphene at early (e and g) and late (f and h) delays at center wavelengths corresponding to the component Gaussians. Component kinetics for pentacene on (i and j) glass and (k and l) graphene at early (i and k) and late (j and l) delays. The colors of the traces in (e–l) match the colors of the associated component Gaussians in (a–d). Excitation was at 519 nm and 50 μJ cm^{-2} fluence.

Published on 23 January 2017. Downloaded by University of Massachusetts - Amherst on 19/07/2017 22:07:59.

Table 2 Parameters describing the Gaussians and exponentials (amplitude; time constant (ps)) used to fit high fluence transient absorption spectra

b (nm)	545.1	551	585	614.1 ± 0.2	630	639 ± 2/ 653.9 ± 0.4[b]	672 ± 0.1/ 676.6 ± 0.1[b]	687.8 ± 0.6
c (nm)	11.1	23	10	19.5 ± 0.2	6	[c]/18.0 ± 0.4[b]	12.91 ± 0.04[c]	[c]
Glass	—	—	—	0.11 ± 0.01; 0.55 ± 0.07	−0.29 ± 0.01; 0.64 ± 0.06	—	—	—
	—	−0.13 ± 0.01; 1.3 ± 0.2	−0.27 ± 0.01; 2.4 ± 0.4	—	—	−0.09 ± 0.03; 150 ± 60	−0.58 ± 0.01; 3.7 ± 0.3	−0.15 ± 0.01; 75 ± 13
	—	−0.04 ± 0.01; 600 ± 200	−0.15 ± 0.01; 1900 ± 400	0.07 ± 0.01; 10000 ± 16000	−0.10 ± 0.01; 3400 ± 2600	[d]; 1900 ± 1700	−0.33 ± 0.01; 2700 ± 300	[d]; 16000 ± 28000
Graphene	−0.63 ± 0.01; 0.48 ± 0.02	[a]	[a]	—	—	—	−0.41 ± 0.01; 0.66 ± 0.02	—
	0.83 ± 0.02; 43 ± 3	[a]	[a]	0.15 ± 0.01; 6.4 ± 0.6	—	−0.27 ± 0.01; 38 ± 2	—	—
	0.61 ± 0.02; 650 ± 30	[a]	[a]	0.13 ± 0.01; 340 ± 30	—	[d]; 16000 ± 10000	−0.566 ± 0.004; 6200 ± 800	—

[a] Unobserved due to overlap with triplet absorption. [b] Glass/graphene. [c] Used same c value. [d] Amplitude for decay matches above rise.

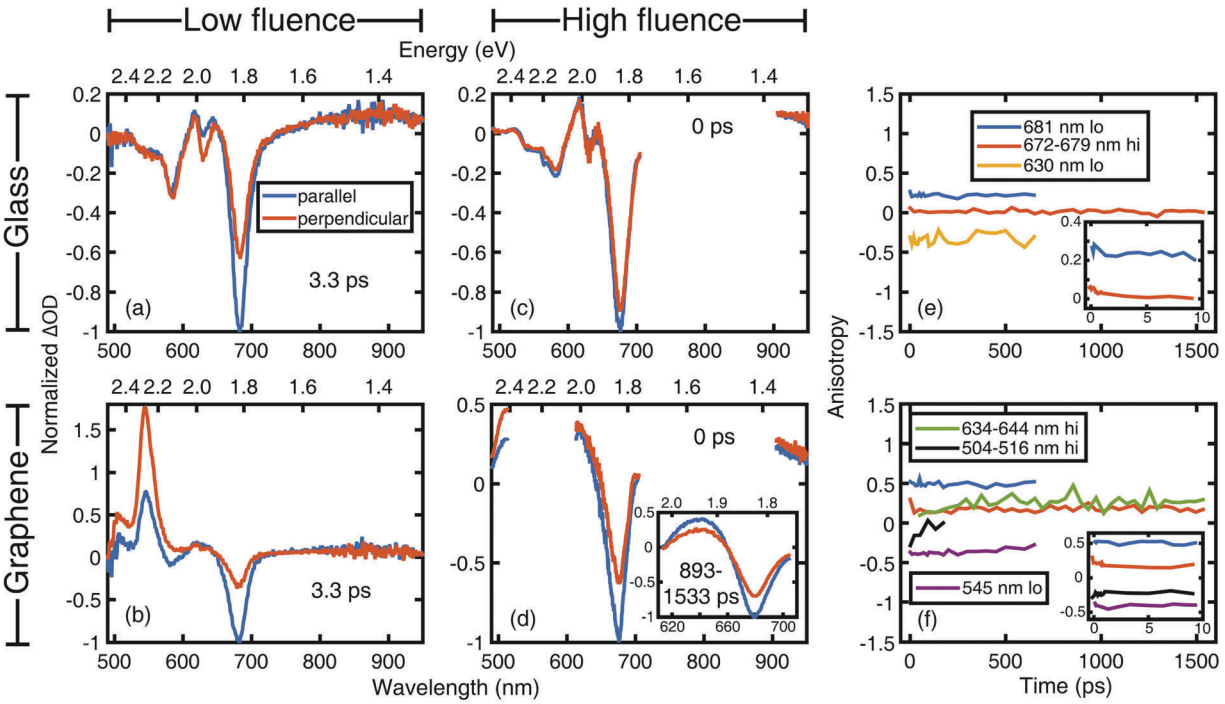

Fig. 6 Transient absorption spectra at parallel (blue) and perpendicular (red) pump–probe polarization for pentacene on (a and c) glass and (b and d) graphene at (a and b) low and (c and d) high fluence. Inset to (d) shows the high fluence spectra for pentacene on graphene at long delays in the region of the 654 and 677 nm features. Transient absorption anisotropy time traces for pentacene on (e) glass and (f) graphene. Insets to (e and f) show select time traces at delays up to 10 ps. Excitation at 560 nm and 35 μJ cm^{-2} fluence.

into the assignments. This equation is slightly different than for a three-dimensional sample, because the orientation of the molecules are only randomized in the (x, y)-plane, as discussed above in Section 3, Theoretical.[27,42,43] As a result, the anisotropy will depend on the tilt of the molecular transition dipoles from the surface normal. From X-ray diffraction, we know that the tilt of the pentacene molecules with respect to the surface normal is maintained among domains.[22]

First, we find further support for assigning the 545 nm peak to triplet excitons. At T = 0 ps, pentacene on graphene has an anisotropy of $S \approx -0.40$ (-0.25) for the 545 nm band at low (high) fluence (Fig. 6e and f). A negative anisotropy is consistent with pumping the S_0–S_1 state and probing the triplet state, since the T_1–T_3 transition dipole moment is perpendicular to that of the S_0–S_1 transition.[25,44–48] Thus, we conclude that the 545 nm transition is indeed due to the formation of triplets for pentacene grown on graphene, at both low and high fluences. Similarly, we conclude that the 630 nm bleach, observed only on glass, arises from coupling and/or energy transfer between the two nearly orthogonal, Davydov-split modes, because it exhibits a negative anisotropy of $S \approx -0.33$ at low fluence.

Second, the anisotropy also helps identify energy transfer through randomization of the transition dipole direction. In a two-dimensional isotropic sample, zero anisotropy can arise

 This journal is © the Owner Societies 2017

Published on 23 January 2017. Downloaded by University of Massachusetts - Amherst on 19/07/2017 22:07:59.

from either randomization in two dimensions or a molecular orientation that has equal absorption for parallel and perpendicular polarizations (see white contour in Fig. 2). The change in pentacene orientation between glass and graphene substrates allows these two situations to be distinguished from one another. If zero anisotropy is found for both molecular orientations, then it must be due to randomization, because otherwise we would measure two different values corresponding to the two different values of θ. As can be seen in Fig. 6a–d, the intensities of the parallel and perpendicular polarized spectra at 614 nm at high fluence are essentially the same, meaning that the anisotropy is zero on both glass and graphene. Therefore, the 614 nm feature corresponds to absorption with a randomized transition dipole moment direction. The 654 nm feature at high fluence on graphene is different, because it has an anisotropy of 0.20 once it grows in (Fig. 6d, inset). $S \approx 0.20$ is also the anisotropy of the 677 nm bleach at long times, which supports the conclusions that the 614 nm feature corresponds to a polaron pair (see the Discussion, Section 5.1) and the 654 nm feature is created by transient heating (see Section 4.4).

Third, the peak at 853 nm also has an anisotropy of zero. We discuss the 853 nm mode in the Discussion, Section 5.1.

4.4 Transient heating and charge generation

A previous report has assigned the absorption features observed for pentacene on glass in the 600–650 nm range to shifting of the absorption spectrum due to transient heating of the sample.[33] To explore whether any of the Gaussians in our fits can be explain by transient heating, we measured the temperature-dependence of the absorption spectrum of pentacene on glass and on graphene and calculated the change in absorption at elevated temperature (see Fig. S5 and following method section, ESI†). Using this difference spectrum and the experimental absorption spectrum at 295 K, we then re-fit our transient absorption data. The fits are shown in Fig. 7 and Fig. S6 (ESI†) for pentacene on glass at low fluence (Fig. S6a, ESI†), pentacene on graphene at low fluence (Fig. S6b, ESI†), and pentacene on graphene at high fluence for T = 900 ps (Fig. S6c, ESI†).

These new fits confirm our assignments of Gaussians to the bleaches and triplets. They also provide new assignments. From the new fits, we conclude that the 639 (glass) and 654 nm (graphene) features at high fluence are created by heating. In Section 4.5 below, we show coherent oscillations that also support the assignment of the 654 nm peak to ground state heating effects. We note that our data is inconsistent with a previous assignment of the 654 nm peak to trapped triplet excitons,[23] because our anisotropy measurements clearly produce a positive anisotropy for this feature (Fig. 6d and f). Thus, the heating experiment assigns two more peaks: the 639 (glass) and 654 nm (graphene) features are caused by transient heating of the molecules due to vibrational relaxation in the electronic excited states.

However, the 614 nm peak can only be partially explained by heating, because a Gaussian must still be included in the fits to create intensity at 614 nm (Fig. 7a and b). Only $<50\%$ of the intensity at 614 nm on glass and none of the intensity at 614 nm on graphene can be attributed to heating. At low fluence, there is less signal left unaccounted for after including heating (Fig. S6a and b, ESI†), in keeping with the blueshifting of the corresponding component Gaussians between the low and high fluence fits of Section 4.2 (623 nm – low fluence and 614 nm – high fluence; see Tables 1 and 2). There is still some contribution from the species giving rise to the 614 nm peak even at low fluence; we return to the assignment of this feature in the Discussion, Section 5.1.

Besides the 614 nm peak, transient heating does not explain the 688 or 853 nm peaks. A possible origin for the 688 nm peak could be a Stark shift created by the formation of free charges. To test for this possibility, we included the previously published electroabsorption spectrum measured for pentacene on glass as an additional spectral component in our fits. Including the electroabsorption spectrum did not improve the fits for pentacene on glass at low fluence nor pentacene on glass at high fluence for short time delays (not shown). However, including the electroabsorption spectrum does provide a better fit for the glass spectrum at high fluence for long time delays, as shown in Fig. 7c, especially at 688 nm. Thus, we assign the 688 nm

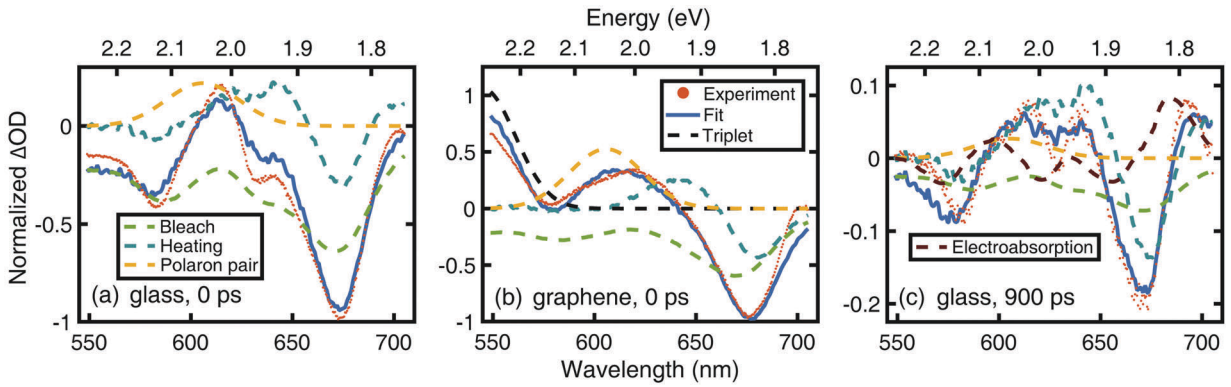

Fig. 7 High fluence transient absorption spectra (red dots) and corresponding fits (blue solid lines) with select spectral components (dashed lines). Pentacene on (a) glass and (b) graphene at T = 0 ps fit with bleaching (green), transient heating (teal), polaron pair (orange), and triplet (black; graphene only) components. (c) Pentacene on glass at T = 900 ps fit with an additional electroabsorption (brown) component.

Published on 23 January 2017. Downloaded by University of Massachusetts - Amherst on 19/07/2017 22:07:59.

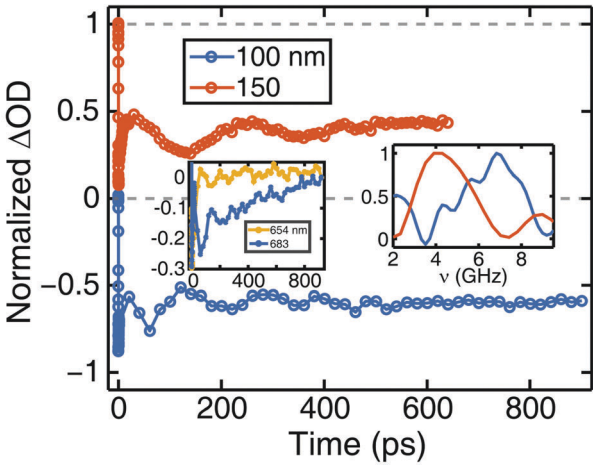

Fig. 8 Transient absorption kinetics at 683 nm for pentacene on graphene with pentacene layers of 100 (blue) and 150 nm (red) thickness with normalized Fourier transforms of the observed oscillations (right inset). (left inset) Comparison of oscillations in transient absorption kinetics at 654 (orange) and 683 nm (blue) for 100 nm thick pentacene on graphene. Curves are offset to zero intensity at T = 920 ps. Excitation at 519 nm, 50 μJ cm^{-2} fluence and 562 nm, 260 μJ cm^{-2} fluence for 100 and 150 nm thickness, respectively.

feature to a Stark shift of the ground state bleach. On the other hand, the features at 614 and 853 nm are not explained by the electroabsorption spectrum; we will assign these peaks in the Discussion, Section 5.1.

4.5 Coherent acoustic phonons

The final piece of data that we present is shown in Fig. 8, in which we observe coherent oscillations in the kinetics of pentacene on graphene at high fluence. The period of these oscillations scale with the thickness of the pentacene film. We assign these oscillations to coherent acoustic phonons created by the impulsive laser excitation.[49] Impulsive oscillations are typically seen in ground state features,[50] and thus help with our assignments. We see oscillations in the 654 and 677 nm peaks, which we have assigned to ground state heating and bleaching, respectively. The oscillation frequencies match the expected frequencies for films of 100 and 150 nm thickness (6.5 and 4.3 GHz, respectively) according to the relation: $\nu = \nu_s/4d$, where ν is the phonon frequency, ν_s is the speed of sound in pentacene ($\sim 2.6 \times 10^5$ cm s^{-1} for pentacene in *p*-terphenyl[50,51]), and d is the film thickness. Oscillations are not seen on glass (Fig. 5f).

5 Discussion

5.1 Assignment of the 614 and 853 nm peaks to bound/free charges

In the Results section, we presented data showing that pentacene on glass and graphene shared largely the same set of features, albeit with different intensities, kinetics, and anisotropies created by the lying-down *versus* standing-up orientation of pentacene on the two surfaces. The 507 and 545 nm features are assigned to triplet excitons. The features at 551, 585, 630, and 681 nm are assigned to bleaching of the ground state. The peaks at 639 (glass) and 654 nm (graphene) at high fluence are created by transient heating. For the 614 nm feature (high fluence) on glass, less than half of the intensity is due to heating, while, on graphene, none of the intensity is caused by heating. The peak at 688 nm on glass at high fluence is created by a Stark shift. This leaves the interpretation of the 614 and 853 nm bands.

We have observed that the 614 nm band is isotropic, is more intense at high fluence, and forms on an instrument-limited timescale with some subsequent decay. We believe that these characteristics are consistent with a polaron pair. A polaron pair is an intermediate state between an exciton and a pair of free polarons (carriers); it is a Coulomb-bound electron and hole located on two adjacent pentacene molecules.[36] Previously published work of pentacene on glass identified a species at ~610 nm, which was assigned to polaron pair absorption according to an electric field-induced transient absorption measurement.[36] Our observation that the 614 nm feature has zero anisotropy is further evidence that this assignment of polaron pairs is correct, because polaron pairs would presumably be generated with equal probability between adjacent pentacene molecules in opposing directions. The larger intensity of the 614 nm peak at high fluence (see Fig. S3, ESI†) is consistent with charge generation occurring as a result of multi-exciton effects, which we discuss in more detail below. Similarly, the appearance of this peak within our pulse duration is consistent with charge generation as a minority loss channel that competes with singlet fission on the <100 fs timescale.[32] We return to this point when we discuss the proposed mechanism of charge generation in Section 5.4.

We now consider the assignment of the broad absorption feature centered at 853 nm. There have been many assignments of species that fall within this frequency range. The T_1–T_2 triplet absorption is commonly reported to appear in this region.[3,31–33,35,41] This assignment is not consistent with our data. We find that the 853 nm band (measured at 906–920 nm at high fluence) has the same intensity for both glass and graphene substrates relative to the bleach and is isotropic according to the anisotropy measurements. If the 853 nm feature was from the T_1–T_2 triplet absorption, which has a well-defined transition dipole direction, we would expect the intensity to vary between the standing-up and lying-down orientations of pentacene on glass and graphene, respectively. Indeed, that is what was seen for the well-known triplet absorption at 545 nm. Another possible assignment for the 853 nm peak is free carrier absorption. Both the pentacene cation and anion have absorptions between 870 and 980 nm, polarized along both the short and long molecular axes, in noble gas matrix absorption spectra.[52] Charge modulation and transient absorption spectroscopy measurements have shown that the pentacene cation has a broad, weak absorption between 750 and 1000 nm[31] and a strong absorption between 1400 and 2000 nm[53] in the solid state.[54] Thus, the frequency range we observe is consistent with pentacene cation (hole) absorption. We note that the lack of orientational dependence for the intensity and the zero anisotropy indicates that this

 This journal is © the Owner Societies 2017

Published on 23 January 2017. Downloaded by University of Massachusetts - Amherst on 19/07/2017 22:07:59.

absorption is isotropic for solid state pentacene, which was not previously reported.

The presence of polaron pairs and charges in the sample is consistent with the interpretation of the 688 nm band, which we have attributed to a Stark shift of the bleach. In measurements of pentacene-C_{60} bilayers,[31] an absorption at $\sim$688 nm was attributed to a Stark shift, because the C_{60} layer provides the appropriate energy offset to split the triplet excitons and generate charges. This same study (532 nm, 120 μJ cm^{-2} fluence pump) reported a reduced electroabsorption in the absence of C_{60}, attributed to possible charge trapping at defect sites or on pentacenequinones at the surface.[31] Furthermore, they noted that this feature increases in intensity with increasing fluence, suggesting possible exciton–exciton annihilation or sequential excitation leading to charge generation.[31,55] These observations are all similar to our own data. Thus, we conclude that the charges that are being generated in our samples are causing Stark shifts exhibited by the 688 nm absorption. We use the 688 nm feature to estimate the number of charges generated at high fluence on glass. Integrating the intensity between 685 and 705 nm for pentacene on glass at 900 ps, we estimate the charge generation yield to be $\sim$3% (Fig. 5b), assuming that there is not a substantial change in the transition dipole moment of the charge state. At low fluence, there is no measurable Stark shift, although we believe some charges are still generated according to the presence of the 853 nm band.

5.2 Evidence for charge extraction by graphene

We have identified the photogenerated species common to both pentacene on glass and graphene to be mostly triplet excitons with a minority population ($\leq$3%) of polaron pairs and free carriers that scales with fluence. Now, we address some of the spectroscopic differences between the two substrates that must be caused by graphene itself.

The kinetics of pentacene on glass and graphene are different, especially for the polaron pair (Table 2). On glass, the polaron pair absorption rises on an instrument-limited timescale, decays on a 0.55 ± 0.07 ps timescale to about half of the initial intensity, and then decays on a 10 ns time scale to about one-third of the initial intensity. On graphene, the polaron pair absorption also rises on an instrument-limited timescale, but then the absorption decays back to baseline on two timescales: 6.4 ± 0.6 and 340 ± 30 ps. The presence of some residual polaron pair intensity on glass and a decay of the polaron pair absorption to baseline on graphene are also reflected in the kinetics obtained from transient heating fits (Fig. S6d and e, ESI†). The structure of the domains is the same, although reoriented, on glass and graphene. Thus, there is no reason to expect a change in recombination rate. Instead, we propose that the additional decay on graphene is due to charge extraction by the graphene. Graphene has been shown to extract charges from pentacene in measurements of a positive surface charge on the pentacene layer following nanosecond excitation at 672 nm.[24] Based on published charge mobilities[11] and triplet exciton diffusion constants,[36] we estimate that both electrons and excitons can reach the graphene interface in tens of picoseconds (for a 100 nm thick film), which matches the experimental timescale for the decay of the 614 nm polaron pair absorption on graphene.

Another difference between pentacene on glass and graphene is the lack of a Stark shift on graphene. This might be because the negative charges are extracted by graphene or it may be that the Stark effect is negligible for the lying-down orientation of pentacene on graphene. Electroabsorption (resulting from the Stark effect) can exhibit lineshapes equivalent to the first or second derivative of the absorption spectrum, depending on whether the change in polarizability or transition dipole moment between the ground and excited states is larger, respectively.[56] On glass, the electroabsorption can take either shape in devices.[57] An electroabsorption spectrum of pentacene on graphene could quantify these effects.

5.3 Effects of domain size/shape on anisotropy/acoustic phonons

The anisotropy, which is larger for pentacene on graphene than on glass (Fig. 6e and f), provides insight into the relative number of grain boundaries in the two samples, because the anisotropy decays when excitons hop between domains.[27] The ground state bleach anisotropy for pentacene on graphene decays weakly within the first couple hundred femtoseconds and remains invariant at $S \approx 0.50$ (0.20) for the entire experimental delay window at low (high) fluence. The bleach anisotropy on glass is much lower at $T = 0$ ps, $S \approx 0.20$ (0.05) at low (high) fluence. At high fluence, the anisotropy decays to zero within tens of picoseconds. The limiting value for the triplet absorption is -0.5 and that for the bleach is 0.5, as derived above in Section 3, Theoretical. There could exist smaller domains at the domain boundaries to allow for multiple reorientations in spite of the diffusion length being on the order of one domain size.[58] The lower anisotropy value on glass is consistent with the presence of more domain boundaries due to the smaller domain size on glass.

In addition to size, the domains on each substrate are distinct in shape, as measured by AFM (Fig. 1e). We propose that the coherent acoustic phonons that give to rise to the oscillations in the 654 and 677 nm peaks (Fig. 8) are supported only on graphene (at high fluence) because of the shape of the domains, which are flatter on graphene. Therefore, acoustic phonons travelling through the domains will reflect and remain in phase. On the other hand, phonons in the terrace-like domains on glass will reflect after travelling different distances and thus dephase on a faster time scale. Therefore, the observation of acoustic waves with frequencies that match the film thickness is a measure of the domain shape.

5.4 Proposed mechanism of charge generation

Previous studies have reported charge generation as a minority loss channel for singlet fission.[30,31,59,60] In this paper, we have presented spectroscopic evidence for $\leq$3% charge generation on a $<$100 fs timescale, with a higher yield at high fluence. A higher yield of charges at high fluence, along with more ground state recovery and lower anisotropy values,[61] are all evidence of multiexciton effects. A previous paper studying the

Published on 23 January 2017. Downloaded by University of Massachusetts - Amherst on 19/07/2017 22:07:59.

fluence dependence of the 853 nm band reported that triplet–triplet annihilation is the dominant decay process for the triplet excitons, noting that the triplet–triplet annihilation rate is expected to be two orders of magnitude faster than the singlet–singlet annihilation rate.[35] Annihilation of the triplets with another species, such as charges, was also ruled out.[35]

Thus, we propose that singlet fission occurs with unity yield of triplet excitons, and the triplet excitons annihilate to produce higher energy singlet and triplet excitons that can dissociate into free carriers.[62] Because double the triplet energy is less than the singlet energy, and probably the ionization energy, charge generation likely requires non-equilibrated triplets, consistent with the low yield. Charge generation may happen from the correlated triplet pair state within $\sim$1 ps of the singlet fission event, as it has been shown that the pair state has a lower exciton binding energy (320 meV)[36] than suggested by the triplet ionization energy.[63] This picture of triplet–triplet annihilation leading to charge generation is consistent with our observation of enhanced charge-related features, namely the polaron pair absorption and Stark shift, at high fluence.

5.5 Comment on the time-dependence of the anisotropy

The appearance of an anisotropy below the theoretical limit within our time resolution suggests that the majority of the exciton hopping is concurrent with singlet fission. At these short times ($<$100 fs), the delocalized triplet pair state has been shown to couple to vibrational modes of the pentacene molecules.[37] Recent work has shown that long-distance (*i.e.* relative to the exciton diffusion length) ultrafast exciton hopping can occur, even when the exciton is small in spatial coherent size, if enhanced by such vibronic coherences.[64] It is possible that the higher energy singlet or triplet excitons generated from the annihilation event are more mobile than the initially generated triplet excitons from singlet fission. Thus, we envision ultrafast hopping of excitons between domains *via* either the delocalized triplet pair state or high energy singlet/triplet excitons, followed by persistence of the remaining excitons on the same domain.

6 Conclusions

In this study, we have used transient absorption spectroscopy and anisotropy to uncover the singlet fission and charge generation dynamics of pentacene on graphene. Since the crystal structure is unchanged aside from being turned on its side, we do not observe any measurable difference in the singlet fission yield between the two morphologies, but the comparison of the data on the two substrates clarifies previous assignments and allows us to identify signatures of charge generation. Anisotropy measurements are also very helpful for assignments. We show that the varied kinetics and anisotropies in the 600–650 nm range at high fluence cannot be explained by solely transient heating. We propose instead significant contributions from polaron pair absorption (614 nm). Our anisotropy data also suggests that, while the 545 nm peak is clearly due to triplet absorption, the 853 nm band appears to have a significant contribution from hole absorption, as this band is isotropic at all times in both samples. We observe evidence of charge extraction by the graphene layer, as reflected by the complete decay of the polar pair absorption on graphene, but not on glass, at high fluence. We observe the signature of a Stark shift on glass, from which we estimate a $\sim$3% yield of charges. We do not observe a similar feature on graphene, but we postulate that more charges should persist to long delays due to electron extraction by graphene. Furthermore, we observe more anisotropy decay in pentacene on glass than on graphene, which is consistent with AFM data showing a larger domain size on graphene. The fact that the graphene-templated film can support coherent acoustic phonons at high fluence is consistent with the difference in domain shape. Our physical picture is that triplet excitons are generated with unity yield *via* singlet fission, followed by the generation of a small population of charges (increasing with fluence) from triplet–triplet annihilation events arising from the correlated triplet pair state. Graphene templating provided a unique opportunity to tune the molecular orientation and gain new physical insights through the corresponding changes in spectroscopic observables. Other organics can be grown on graphene as well,[65] which could provide a similar opportunity to clarify spectral assignments.

Acknowledgements

Funding was provided by the NSF through the University of Wisconsin–Madison Center of Excellence for Materials Research and Innovation (DMR-1121288) and by the Air Force Office of Scientific Research (FA9551-12-1-0063). We acknowledge support from the Defense University Research Instrumentation Program (DURIP) award FA9550-15-1-0320. TJM is supported by the NSF Graduate Research Fellowship Program (DGE-1256259). We acknowledge Ryan D. Kieda for training on the Coherent Legend Elite laser system. We acknowledge Matthew J. Shea and Jialiang Wang for taking the temperature-dependent absorption measurements. MTZ is an owner of PhaseTech Spectroscopy, Inc., which sells femtosecond pulse shapers and 2D spectrometers.

Notes and references

1 W. Shockley and H. J. Queisser, *J. Appl. Phys.*, 1961, **32**, 510–519.
2 M. C. Hanna and A. J. Nozik, *J. Appl. Phys.*, 2006, **100**, 074510.
3 M. B. Smith and J. Michl, *Chem. Rev.*, 2010, **110**, 6891–6936.
4 M. B. Smith and J. Michl, *Annu. Rev. Phys. Chem.*, 2013, **64**, 361–386.
5 J. J. Burdett and C. J. Bardeen, *Acc. Chem. Res.*, 2013, **46**, 1312–1320.
6 J. Lee, P. Jadhav and M. A. Baldo, *Appl. Phys. Lett.*, 2009, **95**, 043303.
7 D. N. Congreve, J. Lee, N. J. Thompson, E. Hontz, S. R. Yost, P. D. Reusswig, M. E. Bahlke, S. Reineke, T. Van Voorhis and M. A. Baldo, *Science*, 2013, **340**, 334–337.

 This journal is © the Owner Societies 2017

Published on 23 January 2017. Downloaded by University of Massachusetts - Amherst on 19/07/2017 22:07:59.

8 N. J. Thompson, D. N. Congreve, D. Goldberg, V. M. Menon and M. A. Baldo, *Appl. Phys. Lett.*, 2013, **103**, 263302.
9 L. Yang, M. Tabachnyk, S. L. Bayliss, M. L. Böhm, K. Broch, N. C. Greenham, R. H. Friend and B. Ehrler, *Nano Lett.*, 2015, **15**, 354–358.
10 J. R. Tritsch, W.-L. Chan, X. Wu, N. R. Monahan and X. Y. Zhu, *Nat. Commun.*, 2013, **4**, 2679.
11 S. B. Jo, H. H. Kim, H. Lee, B. Kang, S. Lee, M. Sim, M. Kim, W. H. Lee and K. Cho, *ACS Nano*, 2015, **9**, 8206–8219.
12 J. Wade, F. Steiner, D. Niedzialek, D. T. James, Y. Jung, D.-J. Yun, D. D. C. Bradley, J. Nelson and J.-S. Kim, *J. Mater. Chem. C*, 2014, **2**, 10110–10115.
13 A. A. Günther, J. Widmer, D. Kasemann and K. Leo, *Appl. Phys. Lett.*, 2015, **106**, 233301.
14 L. Zhang and T. L. Andrew, *Org. Electron.*, 2016, **33**, 135–141.
15 Y. Wan, Z. Guo, T. Zhu, S. Yan, J. Johnson and L. Huang, *Nat. Chem.*, 2015, **7**, 785–792.
16 G. B. Piland and C. J. Bardeen, *J. Phys. Lett.*, 2015, **6**, 1841–1846.
17 D. H. Arias, J. L. Ryerson, J. D. Cook, N. H. Damrauer and J. C. Johnson, *Chem. Sci.*, 2016, **7**, 1185–1191.
18 S. T. Roberts, R. E. McAnally, J. N. Mastron, D. H. Webber, M. T. Whited, R. L. Brutchey, M. E. Thompson and S. E. Bradforth, *J. Am. Chem. Soc.*, 2012, **134**, 6388–6400.
19 J. N. Mastron, S. T. Roberts, R. E. McAnally, M. E. Thompson and S. E. Bradforth, *J. Phys. Chem. B*, 2013, **117**, 15519–15526.
20 R. D. Pensack, A. J. Tilley, S. R. Parkin, T. S. Lee, M. M. Payne, D. Gao, A. A. Jahnke, D. G. Oblinsky, P.-F. Li, J. E. Anthony, D. S. Seferos and G. D. Scholes, *J. Am. Chem. Soc.*, 2015, **137**, 6790–6803.
21 A. Zusan, B. Gieseking, M. Zerson, V. Dyakonov, R. Magerle and C. Deibel, *Sci. Rep.*, 2015, **5**, 8286.
22 L. Zhang, S. S. Roy, R. J. Hamers, M. S. Arnold and T. L. Andrew, *J. Phys. Chem. C*, 2014, **119**, 45–54.
23 H. Marciniak, I. Pugliesi, B. Nickel and S. Lochbrunner, *Phys. Rev. B: Condens. Matter Mater. Phys.*, 2009, **79**, 235318.
24 L. Zhang, S. S. Roy, C. R. English, R. J. Hamers, M. S. Arnold and T. L. Andrew, *ACS Nano*, 2015, **9**, 2510–2517.
25 M. T. Zanni and P. Hamm, *Concepts and Methods of 2D Infrared Spectroscopy*, Cambridge University Press, New York, 2011.
26 R. D. Mehlenbacher, T. J. McDonough, N. M. Kearns, M. J. Shea, Y. Joo, P. Gopalan, M. S. Arnold and M. T. Zanni, *J. Phys. Chem. C*, 2016, **120**, 17069–17080.
27 K. M. Gaab and C. J. Bardeen, *J. Phys. Chem. B*, 2004, **108**, 4619–4626.
28 C. Jundt, G. Klein, B. Sipp, J. Le Moigne, M. Joucla and A. A. Villaeys, *Chem. Phys. Lett.*, 1995, **241**, 84–88.
29 H. Marciniak, M. Fiebig, M. Huth, S. Schiefer, B. Nickel, F. Selmaier and S. Lochbrunner, *Phys. Rev. Lett.*, 2007, **99**, 176402.
30 V. K. Thorsmølle, R. D. Averitt, J. Demsar, D. L. Smith, S. Tretiak, R. L. Martin, X. Chi, B. K. Crone, A. P. Ramirez and A. J. Taylor, *Phys. Rev. Lett.*, 2009, **102**, 017401.
31 A. Rao, M. W. B. Wilson, J. M. Hodgkiss, S. Albert-Seifried, H. Bässler and R. H. Friend, *J. Am. Chem. Soc.*, 2010, **132**, 12698–12703.
32 M. W. B. Wilson, A. Rao, J. Clark, R. S. S. Kumar, D. Brida, G. Cerullo and R. H. Friend, *J. Am. Chem. Soc.*, 2011, **133**, 11830–11833.
33 A. Rao, M. W. B. Wilson, S. Albert-Seifried, R. Di Pietro and R. H. Friend, *Phys. Rev. B: Condens. Matter Mater. Phys.*, 2011, **84**, 195411.
34 W.-L. Chan, M. Ligges, A. Jailaubekov, L. Kaake, L. Miaja-Avila and X.-Y. Zhu, *Science*, 2011, **334**, 1541–1545.
35 A. D. Poletayev, J. Clark, M. W. B. Wilson, A. Rao, Y. Makino, S. Hotta and R. H. Friend, *Adv. Mater.*, 2014, **26**, 919–924.
36 A. R. Srimath Kandada, A. Petrozza and G. Lanzani, *Phys. Rev. B: Condens. Matter Mater. Phys.*, 2014, **90**, 075310.
37 A. A. Bakulin, S. E. Morgan, T. B. Kehoe, M. W. B. Wilson, A. W. Chin, D. Zigmantas, D. Egorova and A. Rao, *Nat. Chem.*, 2016, **8**, 16–23.
38 A. S. Davydov, *Phys.-Usp.*, 1964, **7**, 145.
39 N. J. Hestand, H. Yamagata, B. Xu, D. Sun, Y. Zhong, A. R. Harutyunyan, G. Chen, H.-L. Dai, Y. Rao and F. C. Spano, *J. Phys. Chem. C*, 2015, **119**, 22137–22147.
40 F. Anger, J. O. Ossó, U. Heinemeyer, K. Broch, R. Scholz, A. Gerlach and F. Schreiber, *J. Chem. Phys.*, 2012, **136**, 054701.
41 M. W. B. Wilson, A. Rao, B. Ehrler and R. H. Friend, *Acc. Chem. Res.*, 2013, **46**, 1330–1338.
42 R. D. Mehlenbacher, M.-Y. Wu, M. Grechko, J. E. Laaser, M. S. Arnold and M. T. Zanni, *Nano Lett.*, 2013, **13**, 1495–1501.
43 J. Baumann and M. D. Fayer, *J. Chem. Phys.*, 1986, **85**, 4087–4107.
44 J. G. Müller, J. M. Lupton, J. Feldmann, U. Lemmer, M. C. Scharber, N. S. Sariciftci, C. J. Brabec and U. Scherf, *Phys. Rev. B: Condens. Matter Mater. Phys.*, 2005, **72**, 195208.
45 B. R. Gautam, A. Barrette, C. Mai, L. Yan, Q. Zhang, E. Danilov, W. You, H. Ade and K. Gundogdu, *J. Phys. Chem. C*, 2015, **119**, 19697–19702.
46 L. G. Kaake, J. J. Jasieniak, R. C. Bakus, G. C. Welch, D. Moses, G. C. Bazan and A. J. Heeger, *J. Am. Chem. Soc.*, 2012, **134**, 19828–19838.
47 A. B. Matheson, S. J. Pearson, A. Ruseckas and I. D. W. Samuel, *J. Phys. Lett.*, 2013, **4**, 4166–4171.
48 G. Grancini, D. Polli, D. Fazzi, J. Cabanillas-Gonzalez, G. Cerullo and G. Lanzani, *J. Phys. Lett.*, 2011, **2**, 1099–1105.
49 L. G. Kaake, G. C. Welch, D. Moses, G. C. Bazan and A. J. Heeger, *J. Phys. Lett.*, 2012, **3**, 1253–1257.
50 K. A. Nelson, D. R. Lutz, M. D. Fayer and L. Madison, *Phys. Rev. B: Condens. Matter Mater. Phys.*, 1981, **24**, 3261–3275.
51 J. R. Salcedo, A. E. Siegman, D. D. Dlott and M. D. Fayer, *Phys. Rev. Lett.*, 1978, **41**, 131–134.
52 T. M. Halasinski, D. M. Hudgins, F. Salama, L. J. Allamandola and T. Bally, *J. Phys. Chem. A*, 2000, **104**, 7484–7491.
53 R. H. Friend, M. Phillips, A. Rao, M. W. B. Wilson, Z. Li and C. R. McNeill, *Faraday Discuss.*, 2012, **155**, 339–348.
54 C. P. Jarrett, A. R. Brown, R. H. Friend, M. G. Harrison, D. M. de Leeuw, P. Herwig and K. Müllen, *Synth. Met.*, 1997, **85**, 1403–1404.
55 C. Silva, A. S. Dhoot, D. M. Russell, M. A. Stevens, A. C. Arias, J. D. MacKenzie, N. C. Greenham, R. H. Friend, S. Setayesh

Published on 23 January 2017. Downloaded by University of Massachusetts - Amherst on 19/07/2017 22:07:59.

and K. Müllen, *Phys. Rev. B: Condens. Matter Mater. Phys.*, 2001, **64**, 125211.
56 G. U. Bublitz and S. G. Boxer, *Annu. Rev. Phys. Chem.*, 1997, **48**, 213–242.
57 S. Haas, H. Matsui and T. Hasegawa, *Phys. Rev. B: Condens. Matter Mater. Phys.*, 2010, **82**, 161301.
58 C. Y. Wong, B. L. Cotts, H. Wu and N. S. Ginsberg, *Nat. Commun.*, 2015, **6**, 5946.
59 V. K. Thorsmølle, R. D. Averitt, X. Chi, D. J. Hilton, D. L. Smith, A. P. Ramirez and A. J. Taylor, *Appl. Phys. Lett.*, 2004, **84**, 891–893.
60 S. G. Engelbrecht, M. Prinz, T. R. Arend and R. Kersting, *Appl. Phys. Lett.*, 2014, **105**, 012101.
61 J. Pšenčík, Y.-Z. Ma, J. B. Arellano, J. Hála and T. Gillbro, *Biophys. J.*, 2003, **84**, 1161–1179.
62 D. W. Gehrig, I. A. Howard and F. Laquai, *J. Phys. Chem. C*, 2015, **119**, 13509–13515.
63 A. Köhler and H. Bässler, *Mater. Sci. Eng., R*, 2009, **66**, 71–109.
64 T. Wang, T. R. Kafle, B. Kattel and W.-L. Chan, *J. Phys. Chem. C*, 2016, **120**, 7491–7499.
65 S. Singha Roy, D. J. Bindl and M. S. Arnold, *J. Phys. Lett.*, 2012, **3**, 873–878.

 This journal is © the Owner Societies 2017